

Towards a Spatial Understanding: Transcriptome Profiling of the Tumor Landscape After Ablative Focused Ultrasound Regimens

Timothy Bullock^{1,2}, Frederic Padilla³, Awndre Gamache^{1,2}

Affiliations:

¹Department of Pathology, School of Medicine, University of Virginia, Charlottesville, VA, United States.

²Beirne B. Carter Center for Immunology Research, University of Virginia, Charlottesville, VA, United States.

³Focused Ultrasound Foundation, Charlottesville, VA, United States.

Introduction

Despite recent advances with immunotherapy, metastatic cancer is incurable in most cases. Thus, there is an unmet need to improve both local and systemic therapies for metastatic disease. Focused ultrasound (FUS) therapy stands at the forefront of non-invasive and non-ionizing oncologic treatments, utilizing concentrated ultrasound energy to achieve selective tumor destruction (Padilla *et al.*, 2023).

FUS refers to the convergence of ultrasound, and therefore non-ionizing, waves into a focal volume for non-invasive perturbation of tumor tissues, without damage to tissues outside of the targeted area. The mechanisms of action of FUS are highly versatile, and trigger a broad spectrum of bioeffects that can be thermal or mechanical in nature(Cranston, Leslie and Ter Haar, 2021; Meng, Hynynen and Lipsman, 2021). For ablation of tumor tissues, two main mechanisms of action are thermal ablation and a form of mechanical ablation known as histotripsy(Xu *et al.*, 2024). With thermal ablation, ultrasound energy is delivered at mild intensity, to heat the tissue until temperature of thermal coagulation is reached (typically around 65°C in soft tissues). With histotripsy, extremely high intensities are used, to generate high-amplitude focused ultrasound pulses inducing in mechanical liquefaction of tissues into subcellular debris(Xu *et al.*, 2024).

Interestingly, separate case studies implementing either the histotripsy or thermal focused ultrasound (T-FUS) therapy modalities have shown shrinkage of nontargeted metastases in patients with extensive metastatic disease (Vidal-Jove *et al.*, 2013, 2021). This, along with an abundance of preclinical data, suggests that localized immunogenic effects of FUS-induced cell death within the tumor microenvironment have the potential to promote systemic antitumor immunity(Joiner, Pylayeva-Gupta and Dayton, 2020). Additionally, FUS-induced cell death has been shown to improve antigen availability, dendritic cell activation and maturation, and anti-tumor T-cell responses(Liu *et al.*, 2010; Pepple *et al.*, 2023; Thim *et al.*, 2024). Notably, most of these studies ascertain the transcriptional state, or characterize single cell suspensions, of bulk tumor homogenate. While these approaches have been useful for gleaning the general effects of FUS therapy, they lack sufficient precision to determine how FUS-related immune-sequalae spatially associate with FUS-induced lesions.

T-FUS, Laser-induced thermotherapy, microwave ablation therapy and radiofrequency ablation therapy are all methods that have been utilized to thermally ablate cancer. In all cases, evidence of immunomodulation post treatment has been characterized (Haen *et al.*, 2011). Although there is a dearth of comparative studies to determine whether the quality of immunomodulation differs between these modalities, the core mechanism of action between them relies upon the delivery of energy resulting in heating. In contrast, boiling histotripsy (BH) is a high intensity focused ultrasound ablation strategy that induces lesions through predominantly mechanical tissue fractionation(Khokhlova *et al.*, 2015). Moreover, BH is thought to drive unique immunostimulatory effects which coincide with anti-tumor immunity(van den Bijgaart *et al.*, 2022). The specific inflammatory signatures which promote this immunosensitization, and whether the per ablative zone of BH lesions host the majority of the immune response to tumors, are poorly understood. Quantification and characterization of intratumoral changes in immune cell clustering and innate-immune pathway induction following FUS treatments is necessary to understand potential differences in immunogenicity. Thus, we have performed an initial study that employs spatial transcriptome profiling to determine what underlies the putative differences between these FUS modalities.

Tumor fraction ablation with FUS has been shown to influence immunogenic effects, with sparse-scan regimens (spatially sparse distributed ablation zones) suggested to be more immunogenic than dense-scan regimens (condensed ablation zones)(Liu *et al.*, 2010). This could be due to a higher density of immune cell clusters that form due to the maintenance of viable tumor parenchyma, which may promote the persistence and recruitment of tumor-associated immune cells. These data suggest that the per ablative area around FUS lesions may be a key niche that supports systemic immunity. We investigate the general hypothesis that FUS-induced inflammation primarily modifies immune-sequela within the

periablative zone of FUS induced lesions, and that the distal regions of treated tumors will maintain the transcriptional and cellular landscape of sham-treated tumors. Utilizing a digital spatial transcriptome profiling technique, we examine the identities of immune cells and the inflammatory transcriptome in this area, aiming to clarify how FUS therapy's immunosensitizing byproducts are spatially distributed and to assess the potential of enhancing periablative volume for improved adjuvant effects.

The deployment of spatial transcriptome profiling technologies like GeoMX is revolutionizing our understanding of tumor microenvironments (TME). Traditional RNA-seq does not retain information about the original spatial location of cells within the tissue, losing the context of cellular interactions and microenvironments. By facilitating intricate analysis at the cellular level while maintaining information on tissue structure, GeoMX can offer an unprecedented window into the complex interplay between FUS-induced lesions, cancer cells and their surrounding milieu. This technology is particularly adept at dissecting the spatial and morphological intricacies of tumor tissues, providing insights into how different treatment strategies impact the TME. Here, we utilize GeoMX to perform a comparative analysis of the transcriptional variations induced by either BH or T-FUS therapy in contrast to control conditions and determine whether these phenomena are localized to regions around the lesions (Fig. 1A).

Results

In this study we employ the MC38 colorectal adenocarcinoma model. As we are interested in how immune cells are responding to FUS therapy, it is imperative that immune cells are available in the TME to respond. MC38 is the quintessential "hot" tumor murine model and contains diverse and plentiful immune cells available for profiling(Kienzl et al., 2024). Additionally, the fibrous tumor stroma displays limited regions of necrosis, which makes it more amenable to focused ultrasound therapy. MC38 has also been employed in studies which characterize DC activation and tumor control after T-FUS and mechanical-FUS ablative therapy. In this case, mechanical-FUS ablative therapy was observed to have a more potent effect on inducing a stronger anti-tumor response and inhibitory effect on tumor growth after rechallenge(Hu et al., 2007).

Detection of ablation zones and ROI assignment:

GeoMX enables segmentation of morphological markers to spatially partition and interrogate specific regions of interest in a histological context. This enables deep characterization of the transcriptomic signatures that delineate both the discrete cell subsets and inflammatory pathways that describe the TME. Additionally, the acute effects of both T-FUS and BH have been shown to induce potent DAMP induction and immune cell recruitment 24 hours post therapy. Thus, we collected tissues 24 hours post treatment for characterization. To enable the selection of regions of interest (ROI) in tumors were stained for H&E, cleaved CASP-3 or PARP1, and Hsp70 (Figure 1B). Sham, BH, and T-FUS treated tumors display differences in the morphology of their necrotic (PARP1⁺) regions (Figure 1B). Relative to sham, BH samples contain acellular regions (smooth pink area in H&E) surrounded by areas of fragmented nuclei and reduced cell membrane integrity. The T-FUS treated samples do not contain acellular regions but are predominated by areas of fragmented nuclei and reduced cell membrane integrity. These morphological features correspond with what has been published regarding BH and T-FUS treatment modalities (Khokhlova et al., 2011). Hsp70 was used to define the area of influence relating to FUS-induced lesions. ROIs selected around Hsp70⁺ areas were negative for necrotic staining. We refer to these as periablative (peri) versus distal ROIs. The induction of Hsp70 after treatment with both modalities suggests that the lysate produced by BH can induce similar stress response pathways as T-FUS, despite being a predominantly mechanical rather than thermal mode of ablation.

Comparison of peri-ablation and distal ROI after FUS:

To better understand the impact of FUS treatment on the tumor microenvironment, we performed dimensionality reduction and gene expression analyses on the collected ROIs. Dimensionality reduction of collected ROIs demonstrates that FUS-treated samples cluster separately from untreated (**Fig. 2 A-C**). When assessing bulk ROIs, compared to untreated samples, nearly 1000 genes are differentially regulated 24h after tumors are treated with either BH or T-FUS (**Fig. 2 D**). Gene Ontology (GO) analysis shows the upregulation of RNA processing, regulation and biogenesis pathways localized to the nucleus and promoting translation (**Fig. 2 E**).

We hypothesized that the periablative areas would have distinct transcriptional profiles from distal regions. Surprisingly, dimensionality reduction analysis revealed no unique clusters between these regions. Moreover, there were minimal differentially expressed genes between periablative and distal regions of both BH and T-FUS treated tumors (**Fig 3 A-D**). This data suggest that the transcriptional milieu is somewhat consistent throughout the tumor after FUS treatment. This

may reflect a broad sphere of influence of DAMPs released by the primary lesion, or the activity of FUS away from the biologically discernable ablative/peri-ablative regions.

Estimates of acute inflammation:

A potent inflammatory response has been reported in response to T-FUS in a 4T1 murine breast cancer model in the form of upregulation of innate immune sensor genes and genes encoding for the pro inflammatory cytokines IL-6 and IL-1 β , as well as other inflammasome-related genes 24 hours post treatment (Fite et al., 2021). We looked at gene expression of inflammasome-related genes and discovered that most genes, including *IL-6* and *IL-1 β* , displayed no difference, or a trending decrease, relative to sham controls, except for *txn1* (**Sup_inflammasome A and B**). These data suggest that sham tumors may already be in a heightened state of inflammasome activity that cannot be further augmented in response to BH or T-FUS therapy.

Cellular deconvolution analysis suggests alterations in T cell and macrophage populations after FUS:

MC38 has also been well characterized in the context of the spatial technologies and analysis pipelines that we have employed(Chen et al., 2017). The publicly available scRNASeq data has been optimized for cell type deconvolution in this context, which enable the estimation of immune cell proportions and abundance within ROIs. Cell deconvolution analysis revealed a significant increase in Th17 T cells in treated tumors (**CellDecon A-B**). However, no difference was seen between peripheral and distal regions (**CellDecon C-D**). Interestingly, we also observed a trending increase in the proportion of activated dendritic cells, M0 and M2 macrophages, and CD8 T cells in the peripheral regions of treated tumors (**CellDecon C-D**). These cells play crucial roles in antigen presentation, tumor killing, and the initiation of adaptive immune responses, hinting at a potentially more conducive environment for immune-mediated tumor suppression in these areas. In contrast, there was a trending reduction in Th2 cells, Mast cells, monocytes, and M1 macrophages, which could reflect a shift away from certain anti-inflammatory responses. This reduction may also contribute to a more balanced immune milieu, possibly curtailing the recruitment of cells that may otherwise support tumor growth or suppress effective antitumor immunity. Overall, these findings highlight the dynamic alterations in the tumor immune environment following treatment, suggesting a reprogramming towards a milieu potentially more favorable for antitumor immunity.

The molecular mechanisms underlying FUS-induced tissue damage and its effects on the tumor microenvironment are poorly understood. Our studies, and those of others, have shown that T-FUS can induce tumor ablation by causing coagulative necrosis in the treated area. Whereas BH leads to acellular debris and subsequent necrosis of the surrounding region (Khokhlova et al., 2011). The quality of peripheral inflammation produced T-FUS and BH has yet to be characterized. T-FUS and BH samples exhibit evidence of clustering, with the pronounce effects occurring along PC3 in the PCA analysis (**Fig 4A**). With the described cutoffs, there are around 200 differentially expressed genes between T-FUS and BH (**Fig 4D**). GO analysis again shows upregulation of mRNA processing pathways in BH compared to T-FUS (**Fig. 4 E**). Whereas, T-FUS shows upregulation of growth factor signaling pathways

Discussion:

We anticipated that FUS-induced inflammation would primarily modify immune-sequela within the peri-ablative zone of FUS induced lesions, as defined by HSP70 expression. Moreover, we also hypothesized that the distal regions would phenocopy what is seen in the sham state. Contrary to this hypothesis, we found that even though treated tumors elicited unique transcriptome profiles from shams, there was minimal variance in gene expression between peripheral and distal regions of treated tumors, underscoring a uniform transcriptional response to FUS modalities across the tumor landscape. This suggests a more complex interaction between treatment and tumor biology than originally anticipated. Systemic effects of tissue injury could explain why the effects of localized tissue injury from these treatments radiate across the entire tumor and do not simply result in a return to the baseline state observed in sham tissues. It is known that acute tissue injury can result in the release of various DAMPs that can systemic effects, such as IL1b. Additional research into the dose-response relationship and temporal dynamics of FUS-treated tumors are needed to further clarify the mechanistic basis for this phenomenon.

Both modalities elicited the induction of similar gene pathways related to RNA processing and ribosome biogenesis. Ribosome biogenesis is a critical, multi-step cellular process responsible for constructing ribosomes, the protein synthesis machinery of the cell (Wang et al., 2021). And this underlies general physiological function of all cell processes. In tumor cells, ribosome biogenesis is dysregulated and contributes to their heterogenous nature, as well as promoting tumor growth and expansion (Zisi, Bartek and Lindström, 2022). The activation of these pathways could signify a transition in the overall state of the tumor towards growth. In contrast, sham tissues displayed gene expression profiles that are associated with regulation of inflammatory responses, production of cytokines, and DAMP pathway activation. It is

possible that treatment with BH and T-FUS both resulted in the eradication and subsequent suppression of these active processes. Thus, the changes induced by both modalities may provide a unique opportunity to intervene with drugs that specifically target ribosome biogenesis pathways.

TH17 cells lack robust cytotoxic capabilities and are thought to exert their anticancer effects indirectly by aiding the arrival of effector tumor suppressive immune cells(Kryczek *et al.*, 2009). Indeed, IL-17 is linked with an increase in tumor-infiltrating IFNy+ T cells. Specifically, TH17 derived IL-17 and IFNy work together to boost the secretion of CXCL9 and CXCL10 chemokines by cancer cells(Kryczek *et al.*, 2009). These chemokines are crucial for attracting immune cells, such as T cells and NK cells, to the tumor site. The distal region of T-FUS treated tumors displayed a significant increase in CXCL9 transcripts relative to peripheral regions (**Fig. 3 D**). Additionally, a trending increase was observed for CXCL10 expression in treated tumors relative to shams(**Sup_inflamasome B**). The extent to which TH17 cells influence this distinct expression pattern remains an open question, highlighting a potential avenue for further research to fully understand the mechanisms of TH17 cell involvement in tumor immunity.

Heat shock proteins (Hsps) are a group of chaperone proteins that are synthesized in response to cellular stress, such as heat or radiation. Hsp70 is one of the most studied members of this family and has been shown to play a crucial role in protecting cells from stress-induced damage(Daugaard, Rohde and Jäättelä, 2007; Radons, 2016). Interestingly, we found that FUS-induced lesions exhibit an edge of Hsp70 expression 24 hours after treatment, whereas the necrotic areas of sham tumors do not exhibit this expression profile (Figure 1B). The upregulation of Hsp70 in the edge of FUS-induced lesions suggests that this region is undergoing cellular stress and attempting to protect itself from further damage. This response may be triggered by the release of intracellular contents from the necrotic cells, which can activate the immune system and lead to the recruitment of inflammatory cells to the site of injury. Additionally, Hsp70 expression may contribute to the clearance of damaged proteins and organelles from the damaged cells, thus promoting tissue repair and regeneration. Surprisingly, although Hsp family members were detected in greater abundance in BH and FUS treated tissues relative to shams, there was no detected restriction of expression between peripheral and distal localizations (**Sup_HSPA**). This is despite the clear margins of Hsp70 expression around the tumor. This data suggests that Hsp70 may be post transcriptionally regulated in a way that prevent epitope accessibility in the distal regions of the tumor. Nonetheless, the observation of Hsp70 expression at the edge of FUS-induced lesions provides important insights into the molecular mechanisms underlying FUS-induced tissue damage and the potential role of Hsp family members in tissue repair and regeneration. Further investigation is needed to elucidate the precise mechanisms by which FUS induces cellular stress and Hsp70 expression, as well as to explore the therapeutic implications of these findings.

Nonthermal histotripsy tumor ablation has been shown to promote abscopal response and DC activation that enhances cancer immunotherapy(Qu *et al.*, 2020; van den Bijgaart *et al.*, 2022). Additionally, inoculation with cell-free tumor debris created by histotripsy, unlike those made by radiation or freeze/thaw methods, offers some degree of immunity against implanted tumors(Pepple *et al.*, 2023). The data indicate that mechanical histotripsy produces a distinct type of tumor debris, which in turn prompts a different immune response compared to that following T-FUS. Thus, it is surprising that there is a significant overlap between the genes that were upregulated between modalities in this study. Although boiling histotripsy resulted in primarily a mechanical ablation, it is possible that the thermal component of this therapy may be enough to alter the tumor debris in a similar way as T-FUS. Treatment with BH has been shown to create a paste of tumor debris during over treatment (Khokhlova *et al.*, 2011). Here, short pulses (<5ms) were used which theoretically should not induce thermal phenomena (Wang *et al.*, 2013). Further investigation of this this modality is needed to determine if the lesions induced are devoid of thermal phenomena.

Limitations:

This study comes with several limitations. The instrumentation used differs from that used by other groups, which could lead to different physical phenomena hindering the triangulation of treatment parameters that lead to similar bioeffects. We used a tumor model that is known to be well infiltrated and has a high baseline of immune activity relative to most other models studied. This study focuses on a single timepoint. While we chose a timepoint that has been commonly characterized in the field, there is a lack of temporal nuance to the study that is likely necessary to fully appreciate the bioeffects of FUS therapies. Given these constraints, it's imperative to approach the interpretations and broader applications of our findings with caution, acknowledging that further studies, encompassing diverse instrumentation, tumor models, and multiple timepoints, are essential to comprehensively understand the bioeffects and therapeutic potential of FUS therapies.

Methods:

Mice and Tumor Model.

C57BL/6J mice (Jackson Laboratory) were maintained at the University of Virginia under specific pathogen-free conditions. Mouse experiments were performed in accordance with the Animal Welfare Act and approved by the University of Virginia Institutional Animal Care and Use Committee. Parental MC38 cells (*Kerafast*:ENH204-FP) were implanted subcutaneously in PBS.

Focused Ultrasound Therapy.

FUS treatments were delivered using an in-house designed system at the University of Virginia (**Figure**). It is composed of 4 single elements focused transducers (Sonic Concept), confocally aligned, each of 33mm diameter and 55mm radius of curvature, for a total equivalent aperture of 105mm. The focal zone at -6dB was measured with a needle hydrophone to be roughly spherical, with a width of 1mm and length of 1.2mm, for a volume less than 1mm³.

For targeting, a high-resolution imaging array (MS200, center frequency 30MHz, Visualsonics) is housed at the center of the probe, so that the focal spot is contained within the imaging plane. The therapeutic system is completed with 3D mechanical stages controlled by an Arduino, and driven by a user interface developed in Matlab for treatment planning and for performing the treatment. The animal is positioned above the water bath on a plane holder with a hole in its center where the tumor is positioned.

For thermal ablation, the four transducers are driven simultaneously by a function generator and a power amplifier (E&I, 200W), delivering a total of 13W (about 10W acoustics) for 7s per treatment point, resulting in a 75C peak temperature as measured by thermocouple.

For boiling histotripsy treatment, the transducer were connected to a four-channel power amplifier (TPO, Sonic Concept) delivering 115W per channel (460W total), and driven with 5ms pulses at a PRF of 2HZ for 30s (resulting in 60 pulses per treatment point).

For each of the two FUS modalities, a volume of approximately 40% of the tumor was treated in each case.

Digital spatial profiling.

The GeoMx® DSP platform (NanoString Technologies, Seattle, WA, USA) was employed for spatial transcriptome profiling of murine colon adenocarcinoma(Merritt *et al.*, 2020). GeoMX spatial profiling was performed on 5μm sections cut from FFPE tissues, deparaffinized and rehydrated on glass slides. Tissue sections were then incubated with the murine whole transcriptome analysis(WTA) panel.

To enable ROI selection, slides were stained with, cleaved CASP-3 or PARP1, and Hsp70. H&E slides were assessed for smooth pink acellular regions surrounded by areas of fragmented nuclei and reduced cell membrane integrity, which is indicative of BH, or fragmented nuclei and reduced cell membrane integrity which is indicative of T-FUS. These morphological features correspond with what has been published regarding BH and T-FUS treatment modalities and were characterized by a pathologist.

Following slide scanning, flanking H&E, cleaved-PARP1 and Hsp70 stained tissue sections were examined to identify suitable areas for ROI placement. Circular or polygonal ROIs containing approximately 1600 cells were selected in the tumor periphery (distal), directly adjacent to FUS lesions(proximal), or in areas of necrosis. ROIs in each niche, proximal or distal, were placed to sample multiple regions of similar characteristics. Areas of necrosis that were sampled did not yield significant information. After barcode collection, samples underwent NGS sequencing (NovaSeq S4- output of ~2250M reads/lane (Illumina)) at the University of Minnesota.

Counts were normalized on the GeoMx® instrument to the third quartile for each target. As a higher expression cutoff can lead to less statistical noise, an expression cutoff of 30 counts and LOQ of 2 was employed to enhance statistical acuity (Rachid Zaim *et al.*, 2020). PCA, tSNE, and UMAP dimensionality reduction was run on the GeoMx® DSP platform using the DimReduction.R script V1.2. To assess expression differences across tissue sites, a linear mixed model (LMM) was applied, accounting for the variable number of ROIs per specimen. The Benjamini-Hochberg method corrected p-values to

control the false discovery rate, with results presented as a volcano plot. A fold change cutoff of 1.2 was employed to determine differentially expressed genes.

Cell type deconvolution was performed with the GeoMX DSP software script SpatialDecon_plugin.R V1.3. The deconvolution matrix was derived from a dataset that specialized for both RNA hybridization data and murine immune cells in the context of C57BL/6 mice and MC38 tumors (Chen *et al.*, 2017).

Pathway enrichment analysis was performed with EnrichR-KG (Chen *et al.*, 2013; Kuleshov *et al.*, 2016; Xie *et al.*, 2021).

Data Availability:

Text files of raw data and sample information of the NanoString GeoMx DSP have been deposited at the gene expression omnibus: Uploadinprogress

Should further details be needed to reinterpret the data presented in this paper, they can be obtained by reaching out to the primary contact upon request.

Acknowledgments:

This work was supported by Biorepository and Tissue Research Facility which is supported by the University of Virginia School of Medicine, Research Resource Identifiers (RRID): SCR_022971.

This work was supported by the Spatial Biology Core at the University of Virginia. This work used the GeoMx in the University of Virginia School of Medicine Spatial Biology Core Facility, RRID:SCR_023281

We thank Dr. John Hossack for allowing us to utilize the Vevo 2100 imaging system.

This work was supported by the Focused Ultrasound Foundation.

Figure Legends:

Figure 1: Experimental Design and Histological Analysis of Treated Tumors

(A) Schematic overview of the study design for spatial transcriptome analysis. (B) Representative histological and immunohistochemical analyses of sham, BH, or T-FUS treated tumors. Images show H&E staining alongside cleaved-CASP3 and Hsp70 immunohistochemistry, highlighting the distinct necrotic and stress response patterns induced by each treatment modality.

Figure 2: Gene Expression Alterations Induced by Therapeutic Ultrasound Modalities

(A-C) Dimensional reduction plots (PCA, tSNE, UMAP) comparing gene expression profiles of sham, BH, or T-FUS treated tumor regions 24 hours post-treatment. (D) Volcano plot showcasing genes differentially expressed in treated tumors relative to sham controls, highlighting in red those with an adjusted p-value < 0.05 and a fold change > 1.2. (E) Gene Ontology (GO) analysis of upregulated genes.

Figure 3: Transcriptional Profiles of Peripheral and Distal Tumor Regions Following Treatment

(A-C) Dimensional reduction plots (PCA, tSNE, UMAP) comparing gene expression profiles between peripheral and distal regions within sham, BH, or T-FUS-treated tumors. (D) Volcano plot showcasing genes differentially expressed between peripheral and distal regions, highlighting in red those with an adjusted p-value < 0.05 and a fold change > 1.2.

Figure 4: Differential Gene Expression and Pathway Activation in Peripheral Regions of BH vs. T-FUS Treated Tumors

(A-C) Dimensional reduction plots (PCA, tSNE, UMAP) comparing gene expression profiles between peripheral regions of tumors treated with BH or T-FUS, compared to sham. (D) Volcano plot showcasing genes differentially expressed between BH or T-FUS-treated tumors, highlighting in red those with an adjusted p-value < 0.05 and a fold change > 1.2. (E) GO analysis for differentially expressed genes.

References:

van den Bijgaart, R.J.E. *et al.* (2022) "Mechanical high-intensity focused ultrasound creates unique tumor debris enhancing dendritic cell-induced T cell activation.", *Frontiers in Immunology*, 13, p. 1038347. doi:10.3389/fimmu.2022.1038347.

Chen, E.Y. *et al.* (2013) "Enrichr: interactive and collaborative HTML5 gene list enrichment analysis tool.", *BMC Bioinformatics*, 14, p. 128. doi:10.1186/1471-2105-14-128.

Chen, Z. *et al.* (2017) "Inference of immune cell composition on the expression profiles of mouse tissue.", *Scientific Reports*, 7, p. 40508. doi:10.1038/srep40508.

Cranston, D., Leslie, T. and Ter Haar, G. (2021) "A Review of High-Intensity Focused Ultrasound in Urology.", *Cancers*, 13(22). doi:10.3390/cancers13225696.

Daugaard, M., Rohde, M. and Jäättelä, M. (2007) "The heat shock protein 70 family: Highly homologous proteins with overlapping and distinct functions.", *FEBS Letters*, 581(19), pp. 3702–3710. doi:10.1016/j.febslet.2007.05.039.

Fite, B.Z. *et al.* (2021) "Immune modulation resulting from MR-guided high intensity focused ultrasound in a model of murine breast cancer.", *Scientific Reports*, 11(1), p. 927. doi:10.1038/s41598-020-80135-1.

Haen, S.P. *et al.* (2011) "More than just tumor destruction: immunomodulation by thermal ablation of cancer.", *Clinical & Developmental Immunology*, 2011, p. 160250. doi:10.1155/2011/160250.

Hu, Z. *et al.* (2007) "Investigation of HIFU-induced anti-tumor immunity in a murine tumor model.", *Journal of Translational Medicine*, 5, p. 34. doi:10.1186/1479-5876-5-34.

Joiner, J.B., Pylayeva-Gupta, Y. and Dayton, P.A. (2020) "Focused ultrasound for immunomodulation of the tumor microenvironment.", *Journal of Immunology*, 205(9), pp. 2327–2341. doi:10.4049/jimmunol.1901430.

Khokhlova, T.D. *et al.* (2011) "Controlled tissue emulsification produced by high intensity focused ultrasound shock waves and millisecond boiling.", *The Journal of the Acoustical Society of America*, 130(5), pp. 3498–3510. doi:10.1121/1.3626152.

Khokhlova, V.A. *et al.* (2015) "Histotripsy methods in mechanical disintegration of tissue: towards clinical applications.", *International journal of hyperthermia : the official journal of European Society for Hyperthermic Oncology, North American Hyperthermia Group*, 31(2), pp. 145–162. doi:10.3109/02656736.2015.1007538.

Kienzl, M. *et al.* (2024) "Comparative study of the immune microenvironment in heterotopic tumor models.", *Cancers*, 16(2). doi:10.3390/cancers16020295.

Kryczek, I. et al. (2009) "Phenotype, distribution, generation, and functional and clinical relevance of Th17 cells in the human tumor environments.,," *Blood*, 114(6), pp. 1141–1149. doi:10.1182/blood-2009-03-208249.

Kuleshov, M.V. et al. (2016) "Enrichr: a comprehensive gene set enrichment analysis web server 2016 update.,," *Nucleic Acids Research*, 44(W1), pp. W90-7. doi:10.1093/nar/gkw377.

Liu, F. et al. (2010) "Boosting high-intensity focused ultrasound-induced anti-tumor immunity using a sparse-scan strategy that can more effectively promote dendritic cell maturation.,," *Journal of Translational Medicine*, 8, p. 7. doi:10.1186/1479-5876-8-7.

Meng, Y., Hynynen, K. and Lipsman, N. (2021) "Applications of focused ultrasound in the brain: from thermoablation to drug delivery.,," *Nature Reviews. Neurology*, 17(1), pp. 7–22. doi:10.1038/s41582-020-00418-z.

Merritt, C.R. et al. (2020) "Multiplex digital spatial profiling of proteins and RNA in fixed tissue.,," *Nature Biotechnology*, 38(5), pp. 586–599. doi:10.1038/s41587-020-0472-9.

Padilla, F. et al. (2023) "Guidelines for immunological analyses following focused ultrasound treatment.,," *Journal for immunotherapy of cancer*, 11(11). doi:10.1136/jitc-2023-007455.

Pepple, A.L. et al. (2023) "Spatiotemporal local and abscopal cell death and immune responses to histotripsy focused ultrasound tumor ablation.,," *Frontiers in Immunology*, 14, p. 1012799. doi:10.3389/fimmu.2023.1012799.

Qu, S. et al. (2020) "Non-thermal histotripsy tumor ablation promotes abscopal immune responses that enhance cancer immunotherapy.,," *Journal for immunotherapy of cancer*, 8(1). doi:10.1136/jitc-2019-000200.

Rachid Zaim, S. et al. (2020) "Personalized beyond Precision: Designing Unbiased Gold Standards to Improve Single-Subject Studies of Personal Genome Dynamics from Gene Products.,," *Journal of personalized medicine*, 11(1). doi:10.3390/jpm11010024.

Radons, J. (2016) "The human HSP70 family of chaperones: where do we stand?," *Cell Stress & Chaperones*, 21(3), pp. 379–404. doi:10.1007/s12192-016-0676-6.

Thim, E.A. et al. (2024) "Focused ultrasound ablation of melanoma with boiling histotripsy yields abscopal tumor control and antigen-dependent dendritic cell activation," *Theranostics* [Preprint].

Vidal-Jove, J. et al. (2013) "Complete Responses after Hyperthermic Ablation by Ultrasound Guided High Intensity Focused Ultrasound Plus Systemic Chemotherapy for Locally Advanced Pancreatic Cancer," *Conference Papers in Medicine*, 2013, pp. 1–4. doi:10.1155/2013/586769.

Vidal-Jove, J. et al. (2021) "Liver Histotripsy Mediated Abscopal Effect-Case Report.,," *IEEE Transactions on Ultrasonics, Ferroelectrics, and Frequency Control*, 68(9), pp. 3001–3005. doi:10.1109/TUFFC.2021.3100267.

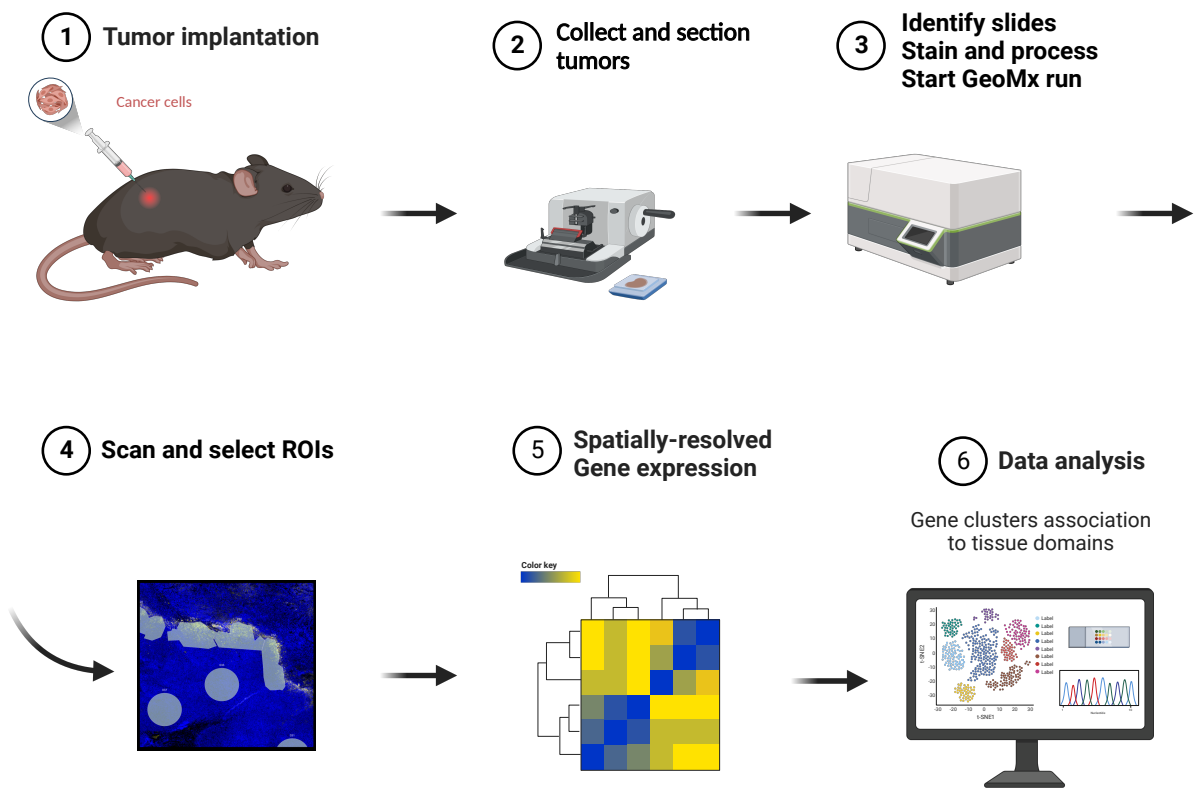
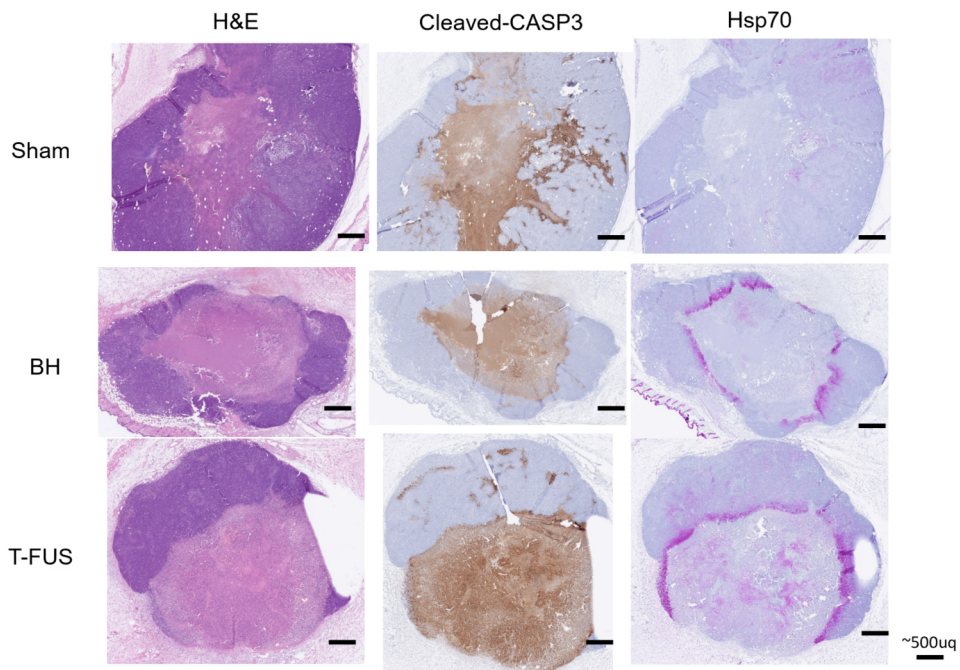
Wang, B. et al. (2021) "Integrated analysis of the roles of RNA binding proteins and their prognostic value in clear cell renal cell carcinoma.,," *Journal of healthcare engineering*, 2021, p. 5568411. doi:10.1155/2021/5568411.

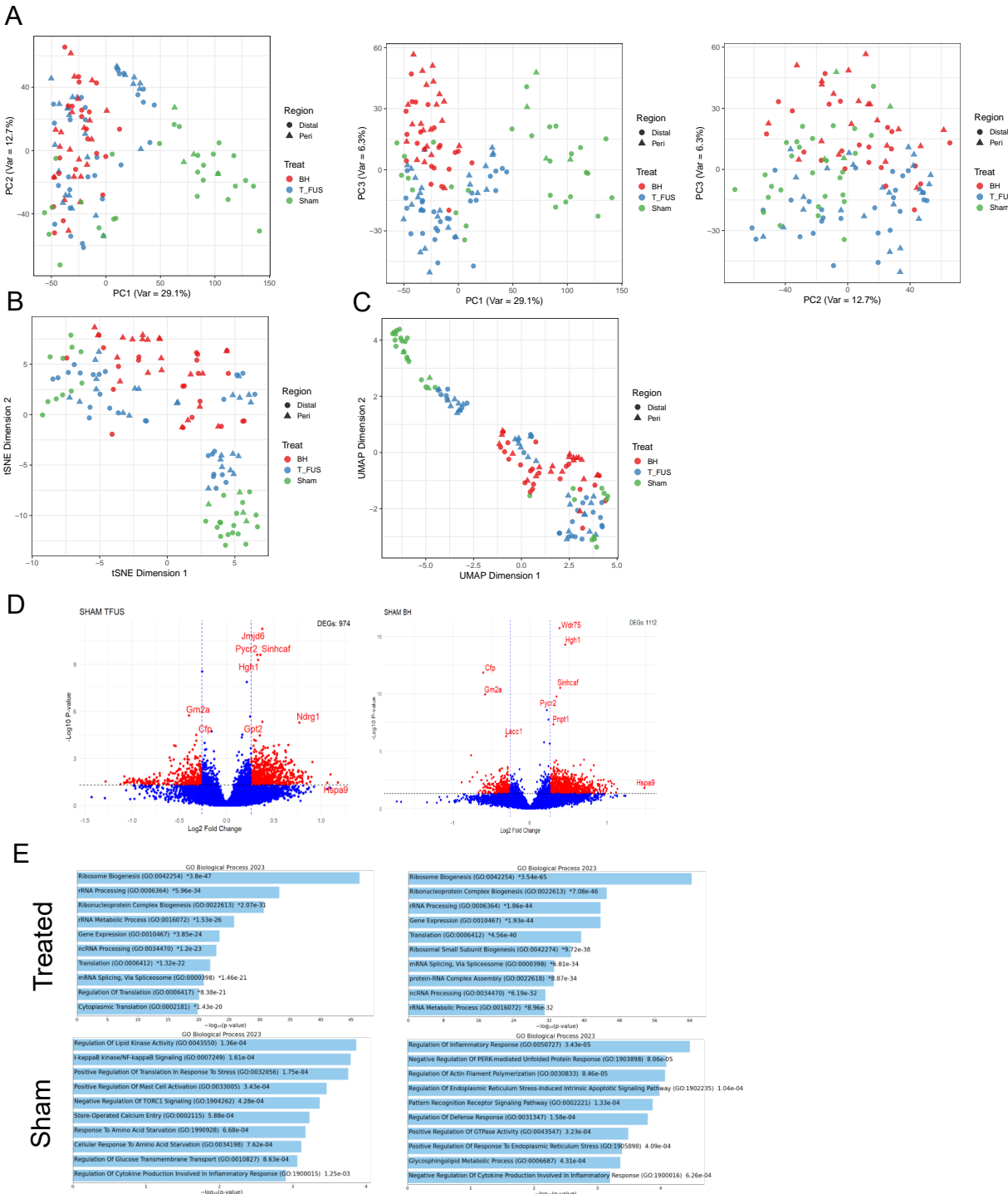
Wang, Y.-N. et al. (2013) "Histological and biochemical analysis of mechanical and thermal bioeffects in boiling histotripsy lesions induced by high intensity focused ultrasound.,," *Ultrasound in Medicine & Biology*, 39(3), pp. 424–438. doi:10.1016/j.ultrasmedbio.2012.10.012.

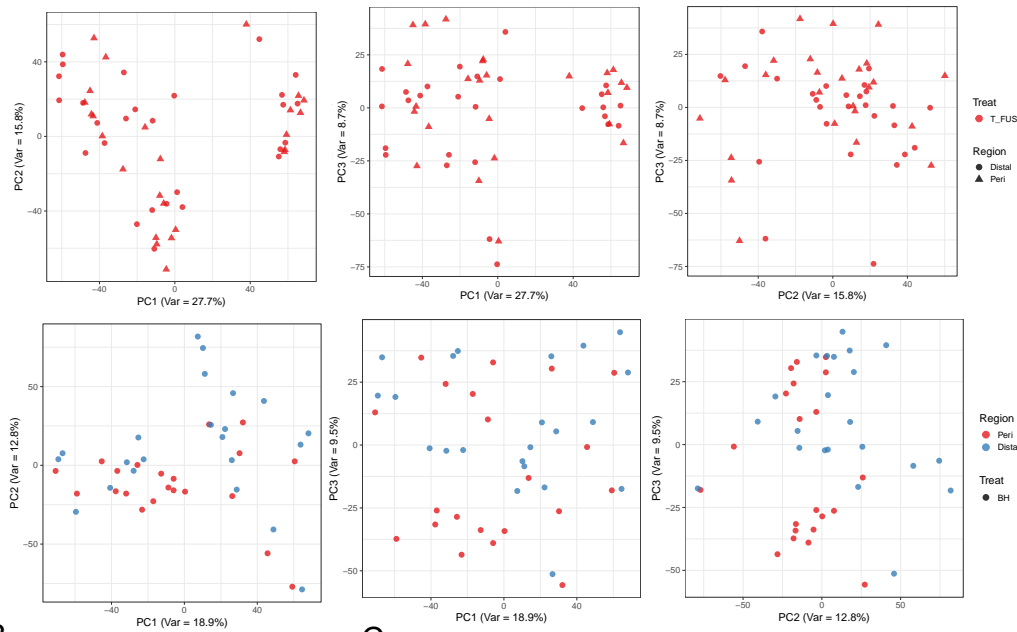
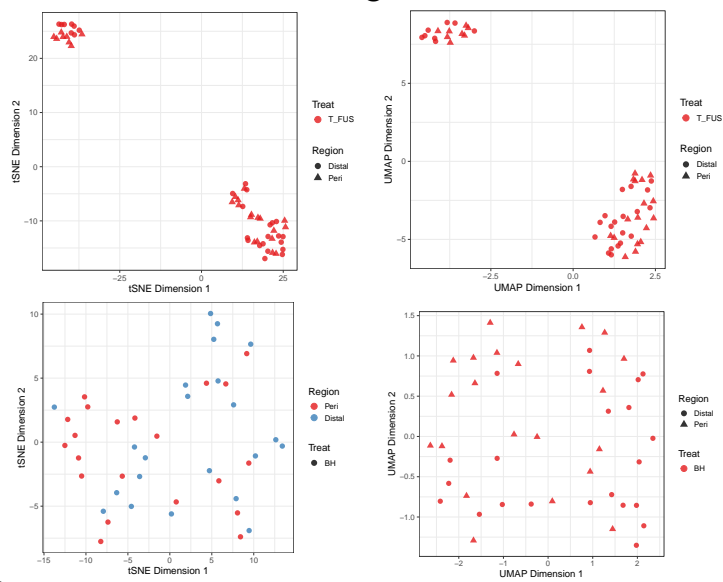
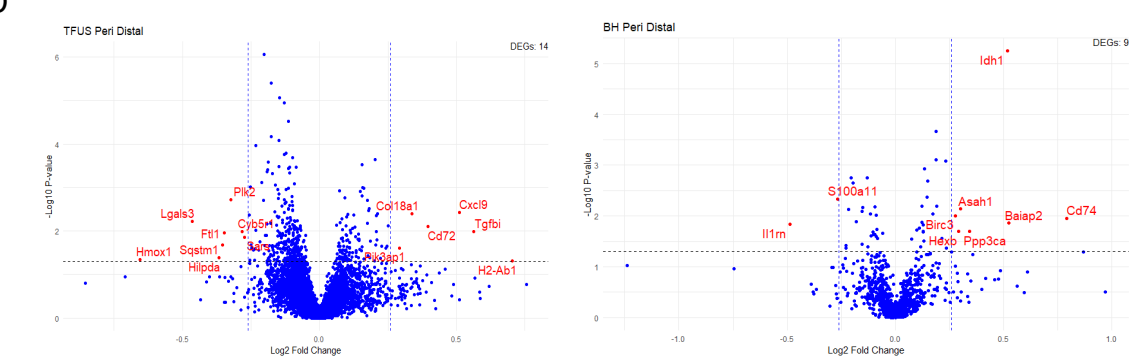
Xie, Z. et al. (2021) "Gene Set Knowledge Discovery with Enrichr.,," *Current protocols*, 1(3), p. e90. doi:10.1002/cpz1.90.

Xu, Z. et al. (2024) "Histotripsy: A Method for Mechanical Tissue Ablation with Ultrasound," *Annual Review of Biomedical Engineering*, 26(1), pp. 141–167. doi:10.1146/annurev-bioeng-073123-022334.

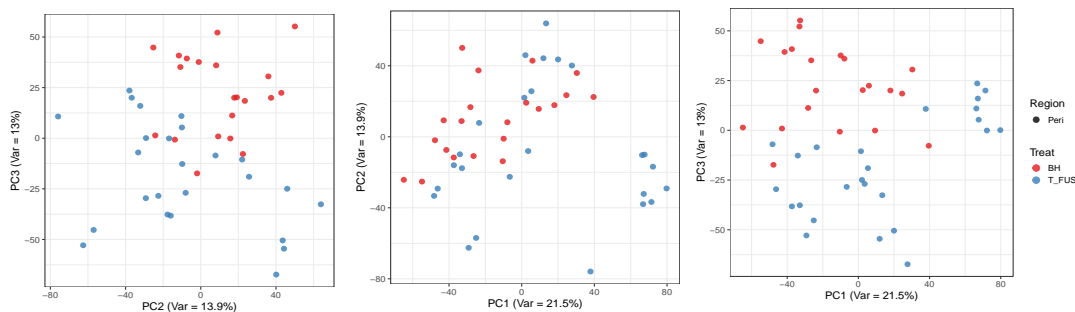
Zisi, A., Bartek, J. and Lindström, M.S. (2022) "Targeting ribosome biogenesis in cancer: lessons learned and way forward.,," *Cancers*, 14(9). doi:10.3390/cancers14092126.

A**B**

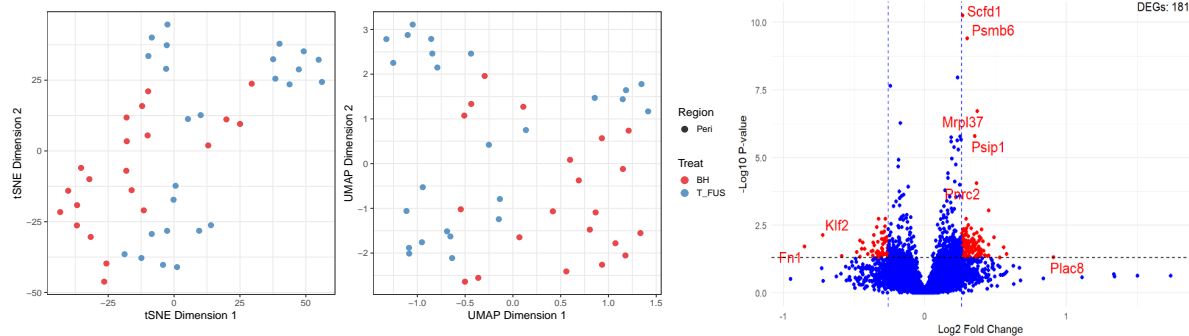


A**B****C****D**

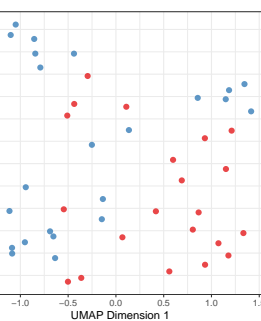
A



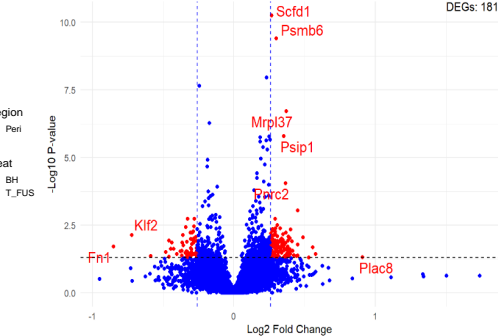
B



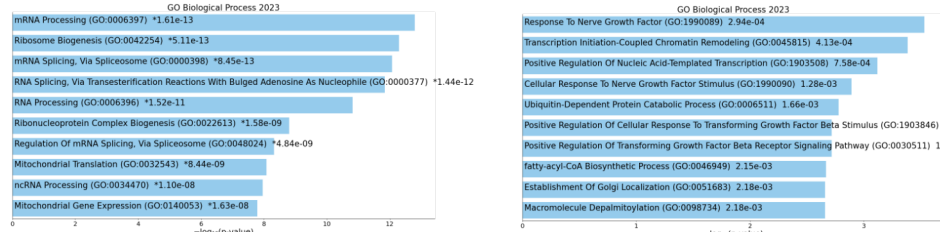
C

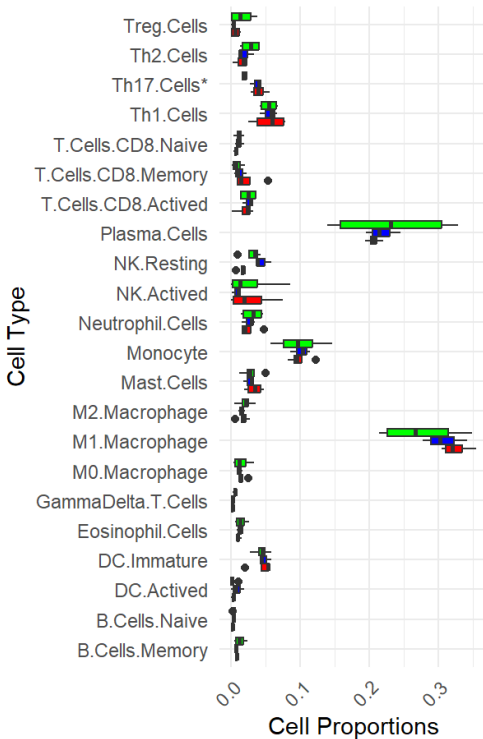
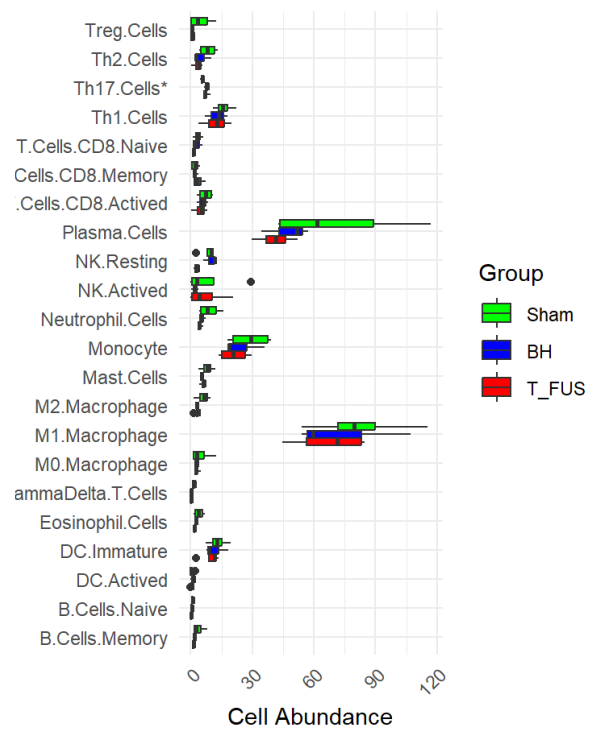
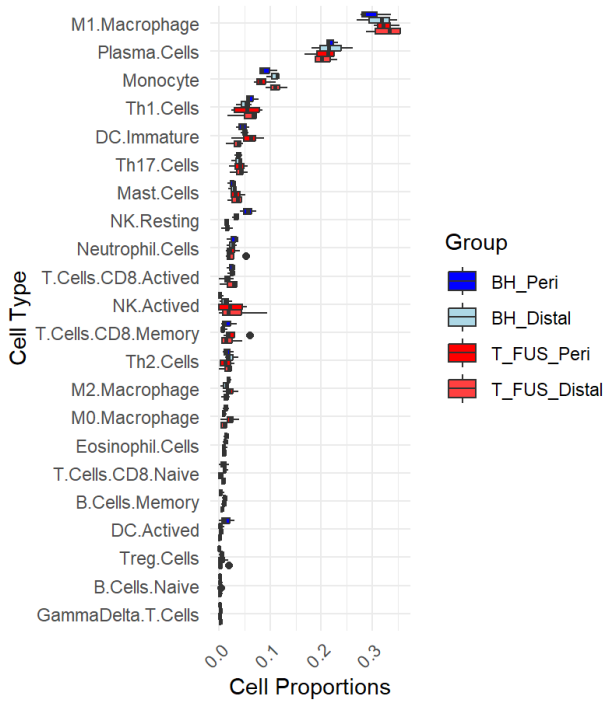
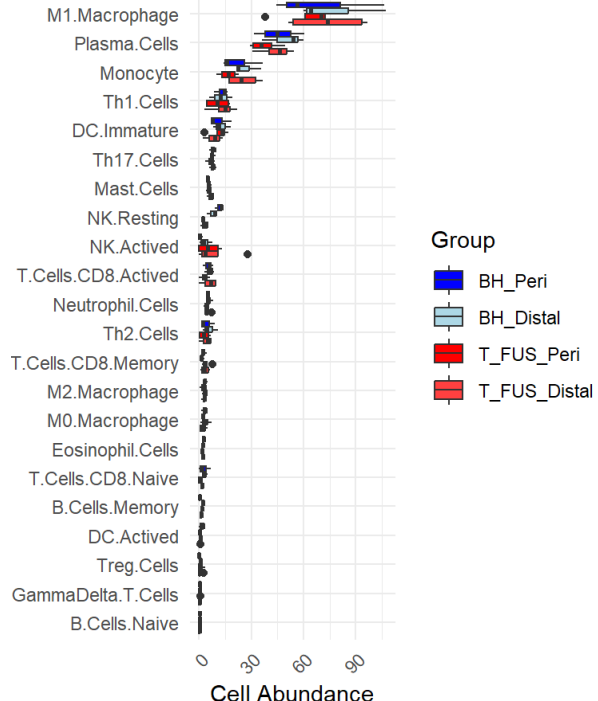


D

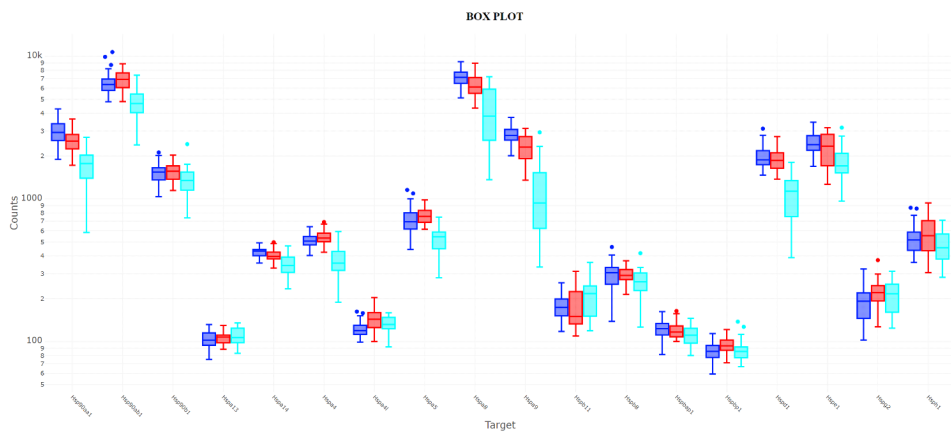


E

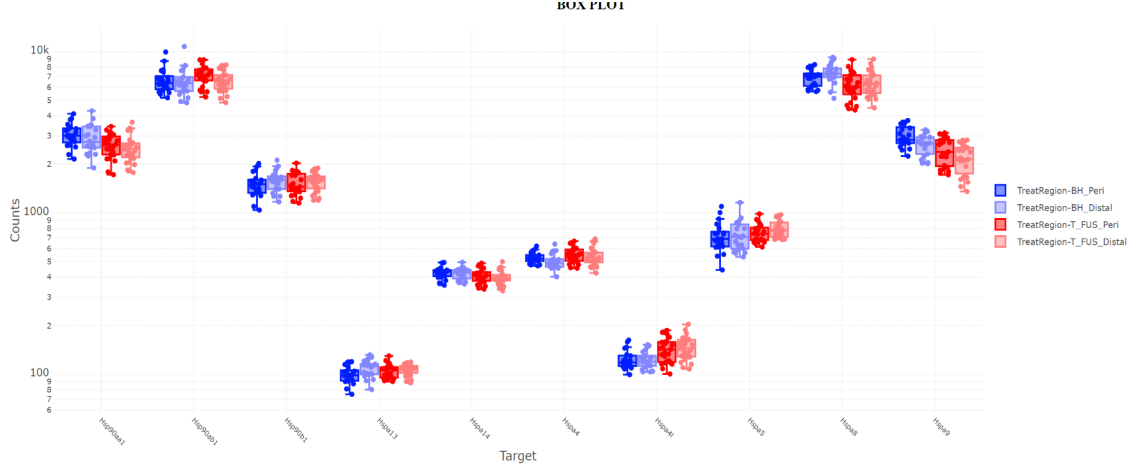


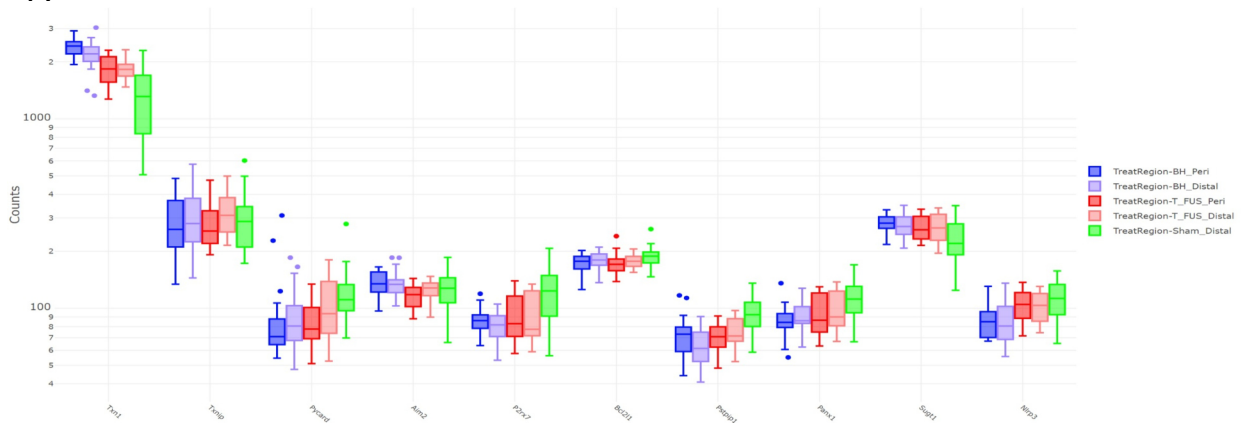
A**B****C****D**

A



B



A**B**